Diffusion and thermal stability of amorphous copper zirconium

Eric C. Stelter* and David Lazarus

*Department of Physics and Materials Research Laboratory, University of Illinois at Urbana-Champaign,
Urbana, Illinois 61801*

Measurements have been made of diffusion and thermal relaxation in amorphous $Cu_{50}Zr_{50}$ samples prepared by melt spinning in vacuum. Diffusion of Ag and Au impurities over the temperature range 317–385 °C was measured by Auger-electron spectrometry (for Ag) and Rutherford-backscattering spectrometry (for Au). Diffusivities of Ag and Au were found to be comparable to values for self-diffusion in crystalline Cu at the same temperatures, but activation energies and preexponential factors for the amorphous alloy are much smaller than those for the crystalline solid. These results suggest that the basic diffusion mechanism for the amorphous alloy may be an extended, liquidlike defect involving 13 or more atoms, rather than the monovacancy well established for crystalline Cu. Thermal relaxation measurements were made in amorphous Cu-Zr to 550 °C by differential scanning calorimetry. The relaxation processes are characterized by a spectrum of activation energies, the lowest of which is essentially the same as that measured for Ag diffusion. The activation energy for crystallization is far larger, implying that the rate-limiting step in the amorphous-crystalline transition is the formation of finite crystallization nuclei, rather than only the diffusional motion of atoms.

I. INTRODUCTION

Amorphous metals, or metallic glasses, are nonequilibrium structures with no long-range crystalline or compositional order. Short-range order present in these materials usually extends only over distances of a few interatomic spacings. The densities of amorphous metals are slightly less than those of comparable crystalline phases, and the structure of these materials is similar to that of a supercooled liquid, often approaching a dense random packing of hard spheres.

Very few diffusion measurements have been made in metallic glasses because of the inherent instability of the amorphous phase. Many of the most stable metallic glasses crystallize rapidly at temperatures of 500 or 600 °C. At lower temperatures, crystallization is preceded by a brief incubation period. Consequently, to study diffusion in these materials, diffusion anneals must be made only for very short times at relatively low temperatures, where atomic motion is limited to a few tens of interatomic spacings.

Measured diffusivities of many elements in both metal-metal (M-M) and metal-metalloid (M-$\mathcal{M}$) glasses fall in a narrow range between values typical for diffusion of small interstitials (e.g., B in Fe) and volume self-diffusion in close-packed crystalline lattices at comparable temperatures.[1] Diffusion measurements to date on M-M glasses are too sparse to permit any precise specification of atomistic mechanisms for these alloys, although some regularities have been observed. In $Ni_{59.5}Nb_{40.5}$, B is found to diffuse faster than Au,[2,3] similar to the behavior in M-$\mathcal{M}$ glasses and crystalline metals. Studies of diffusion of Au, Pt, and Pb in $Ni_{33}Zr_{67}$ show a rough correlation of diffusivity with the atomic volume of the impurity, as measured by its Goldschmidt

radius: Larger atoms diffuse more rapidly and possibly with higher activation energies.[4,5] However, in $Ni_{50}Zr_{50}$, Au diffusion is slower than that of Ni or Cu.[6]

Measurements of diffusion in metallic glasses are often difficult to interpret because the structure of the glass is not fixed like that of a crystalline solid, but is a function of the quenching rate during glass formation and the degree of subsequent thermally induced structural relaxation. Diffusion is generally faster in more rapidly cooled and unrelaxed glasses, which also contain more free volume than more slowly cooled and relaxed samples.

The present study involved measurements of diffusion and thermal relaxation in a single M-M glass, amorphous $Cu_{50}Zr_{50}$. This alloy was chosen for a number of reasons: its structure after quenching is near to ideal random packing;[7,8] it is relatively stable over a considerable temperature range; it eventually crystallizes into a single phase;[9] and it is stable over a fairly large range of compositions. Accordingly, the basic properties of the glass should not be expected to change appreciably with small variations in composition. Since the basis for stability of M-M glasses is more obscure than that of M-$\mathcal{M}$ glasses, it was also hoped that these studies could contribute to a better understanding of the glass-forming ability of M-M alloys.

The amorphous Cu-Zr samples used for this study were prepared by melt spinning under vacuum, as described in the next section. Diffusion was measured for Ag impurities by Auger-electron spectrometry (AES) and for Au impurities by Rutherford-backscattering spectrometry (RBS). Both techniques permit measurement of the effects of atomic motion over a few tens of interatomic spacings. Conventional methods for measurement of diffusion, e.g., by use of radioactive tracers, involve motion of atoms over such large distances—

typically at least tens of thousands of interatomic spacings—that an initially amorphous sample could not be expected to retain its random structure during such a diffusion anneal.

Use of AES and RBS dictates that the motion of some impurity other than a major constituent be studied. Ag and Au, evaporated onto the samples in thin layers, were chosen as "stand ins" for Cu. They are both isoelectronic to Cu, have comparable atomic sizes, are readily soluble in Cu, and diffuse in crystalline Cu at essentially the same rate as Cu. Ag and Au are nearly optimal for study by AES and RBS, respectively, and diffusivities can be derived by direct comparison of the concentration profiles of these impurities between unannealed and annealed samples.

The thermal stability of the $Cu_{50}Zr_{50}$ glass was investigated by differential scanning calorimetry (DSC). Exothermal effects associated with relaxation and crystallization of the as-quenched alloy were measured at several heating rates, permitting calculation of activation energies which could then be compared to those measured for diffusion.

II. EXPERIMENTAL

A. Sample preparation

Samples were prepared from Cu rod of 99.999% purity and Zr slugs of 99.99% purity, excluding Hf, both obtained from the Materials Research Corporation, Orangeburg, N.Y. Since both Cu and Zr oxidize readily, care was taken in all steps of the sample preparation procedure to avoid contamination by oxygen. The Cu rod was cut into short lengths with a jeweler's saw, degreased in acetone, ethanol, and methanol, dried with Freon, and then etched in a 35% nitric acid solution to remove oxidation and other surface contaminants. After etching, the Cu was rinsed in deionized water and alcohol, then dried with Freon. The Zr slugs were received in a sealed container and did not require etching, but were simply degreased and dried before weighing.

Pre-weighed amounts of Cu and Zr were alloyed by electron-beam melting under a vacuum exceeding 5×10^{-7} Torr. The crystalline sample was then homogenized under high vacuum in an induction furnace by repeated melting, turning, and resolidification. After at least three such steps, the alloy was cast into a cylindrical ingot in an oxygen-free high-conductivity (OFHC) Cu mold.

Amorphous $Cu_{50}Zr_{50}$ ribbon was produced with the vacuum melt-spinning rig in the University of Illinois Department of Metallurgy. The alloy ingot was placed inside a quartz tube with a 0.015-in. hole in one end and vacuum melted by induction heating. The liquid metal was then forced through the opening in the tube with purified argon gas in a thin stream onto a rapidly rotating OFHC Cu wheel below, where it was quenched to form a thin ribbon, about 0.001-in. thick and 0.125-in. wide. The base vacuum at the beginning of each run exceeded 2.0×10^{-6} Torr. Subsequent x-ray diffraction examination of the ribbons disclosed no signs of crystallinity.

Quenching rates during melt spinning are estimated to be about 10^6 K/sec. The side of the ribbon in contact with the Cu wheel (the "wheel side") is more rapidly cooled than the opposite side (the "top side").

Before each run, the Cu wheel was polished with 600 grit silicon carbide paper and cleaned with acetone and alcohol to minimize surface contamination of the ribbon. To determine if the quartz tube used in melt spinning was a significant source of oxygen contamination, a slug of $Cu_{50}Zr_{50}$ was placed in a quartz tube, vacuum melted by induction heating, and allowed to solidify. The Cu-Zr did not adhere to the walls of the tube, which showed no signs of erosion. Contamination from the quartz tube was concluded to be minimal.

Ribbon samples were kept in a vacuum dessicator after preparation to minimize subsequent oxidation. Even after several months, there were no visible signs of degradation of ribbon surfaces (which otherwise discolored within a few weeks if kept in air).

B. Diffusion measurements

Short sections of the amorphous ribbon, about $\frac{1}{2}$-in. long, were cleaned in acetone, ethanol, and methanol and placed inside a vacuum evaporator. There, 600-Å-thick films of Ag (for AES measurements) or 40-Å-thick films of Au (for RBS measurements) were deposited under a vacuum of at least 5×10^{-6} Torr. The coated samples were then placed, along with a small chip of $Zr_{87}Ti_{13}$ (which is a more efficient getter than either pure Ti or Zr), inside 5-mm diameter quartz ampoules. The ampoules were purged three times by filling with purified Ar and evacuating before being sealed under a pressure of about 0.3 atmospheres of Ar. The Ar gas was purified by passing it through a furnace containing $Zr_{87}Ti_{13}$ chips at 840 °C. During the sealing operation, the ampoules were immersed in cold water to avoid heating of the samples prior to the diffusion anneal. The seal was formed about 3-in. above the top end of the samples.

Samples were diffused by inserting the sealed ampoules rapidly inside a massive preheated stainless-steel block at the center of a furnace. This method ensured minimal warm-up time in reaching the diffusion temperature (less than 1 min). Samples were held at constant (± 0.5 °C) temperatures ranging from 317 to 385 °C for periods of 300 min (at 317 °C) to 25 min (at 385 °C). At the end of the diffusion anneal, the ampoules were quickly removed from the furnace and quenched in ice water. The Ag- and Au-coated samples were always diffused simultaneously to ensure that they had identical thermal histories. X-ray diffraction measurements made after diffusion anneals disclosed no evidence of crystallization in any of the samples.

C. Concentration profile analysis

The Ag concentration profiles in unannealed and diffused samples were determined by AES, using a Physical Electronics 595 Multiprobe in the University of Illinois Center for Microanalysis of Materials. Auger analysis was done with a 3.0 keV, 40 nA electron beam. The concentration of an element on the surface of a sam-

ple measured by AES is proportional to the peak-to-peak height of the derivative of the characteristic Auger electron emission peak of that element. Concentrations of Ag as a function of depth were obtained by sputtering the surface between Auger scans with a 2.5-keV Ar beam, which removed material at a rate of less than 6.25 Å/min. The sputtering beam formed a crater in the sample surface of about 2-mm diameter. Auger measurements were made on a small, relatively flat region of 1-micron diameter at the center of the crater.

The diffusion of Au was measured by RBS using the Rutherford-backscattering facility at the Center for Microanalysis of Materials. Backscattering spectra were obtained by placing samples in a beam of 2.0-MeV He + ions accelerated by means of a van der Graaf accelerator and measuring the energy spectrum of backscattered He ions at an angle of 174.5° from the incident beam with an energy-dispersive silicon-barrier detector (Ortec BA14-25-10).

A relatively thin film of Au on the surface of Cu-Zr produces a peak in the spectrum of backscattered ions at higher energy than the spectrum resulting from the rest of the sample, and with an energy width about the same as that of the beam. For such thin films, the surface energy approximation is valid: The energy loss per unit distance, dE/dx, and, to first order, the scattering cross section can be taken to be constant. The energy of the backscattered particles from regions of the sample with roughly constant concentration can therefore be readily converted linearly to the depth of the scatterer below the surface.

Because of its high Z and A, Au can be readily detected by RBS in a background of lighter Cu and Zr. As shown in the next section, the spectrum resulting from scattering by Au is well separated from the Zr edge (the heavier element in the glass). Unfortunately, it is not possible to use the same technique to measure Ag diffusion, since Ag is too close to Zr in mass for the spectra to be resolved with any precision. Similarly, while AES is extremely sensitive to Ag and the Ag peak can be resolved without difficulty in the presence of Cu and Zr, the Auger peak from Au is too close to that of Zr to be resolved. Therefore, with the means available, it was not possible to measure the diffusion of both Ag and Au in the same sample by a single microanalytical technique.

The low annealing temperatures and short diffusion times mandated in this experiment resulted in mean diffusion distances not much larger than the limits of resolution of the measurement methods used. Accordingly, the experimental errors inherent in the depth measurements are appreciable, as will be discussed in the following section.

D. Thermal measurements

Exothermal effects resulting from redistribution of atoms during stabilization and crystallization of the $Cu_{50}Zr_{50}$ were measured by differential scanning calorimetry. A DuPont 910 DSC and 1090 Thermal Analyzer in the Center for Microanalysis of Materials were used for these measurements. Samples were placed
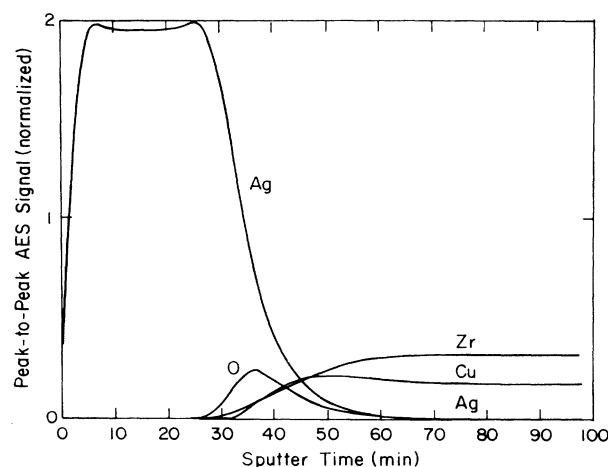

FIG. 1. An AES profile of the Ag/Cu-Zr interface of an unannealed sample.

inside an enclosed cell under an atmosphere of purified Ar, which was renewed at a rate of 25 cm³/min. The Ar gas was purified by passing it through the getter furnace described earlier. Before each run, the DSC cell was evacuated and backfilled three times with Ar to purge it of oxygen. Samples and Al references were nominally 15 mg in weight and were enclosed in Al pans.

The temperature, T_{max}, at which the maximum heat flow occurs from an activated process is a function of the rate, I, at which the sample is heated. As the heating rate is increased, T_{max} increases. The activation energy for the process can be obtained from the slope of a Kissinger plot of $\log(I/T_{max}^2)$ versus $1/T_{max}$.[10]

III. RESULTS

A. Ag diffusion

An AES profile from an unannealed Ag-coated sample of amorphous $Cu_{50}Zr_{50}$ is shown in Fig. 1. Due to the sensitivity of AES to Ag, the amplitude of the Ag profile, shown here as measured, is much greater than
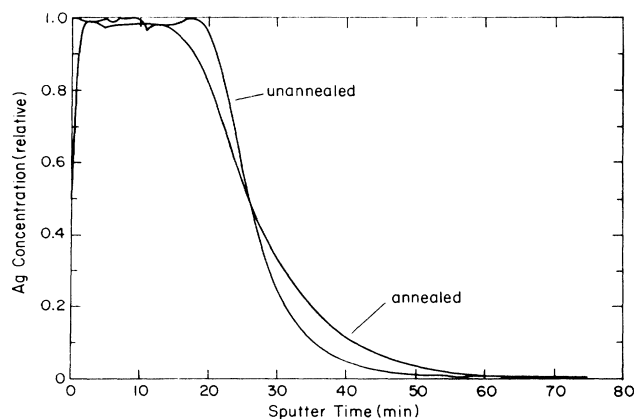

FIG. 2. Concentration of Ag at the Ag/Cu-Zr interface of an unannealed sample and a sample which was annealed at 317.0 °C for 300 min.
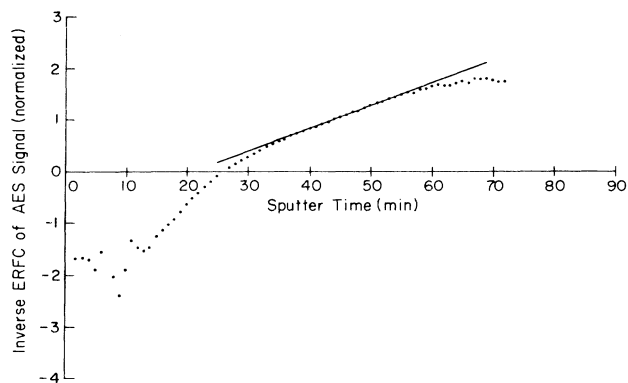
FIG. 3. Plot of the inverse complementary error function of the Ag concentration (normalized to 2) at the Ag/Cu-Zr interface of a sample which was annealed for 300 min at 317.0 °C. The linearity of the curve in the midsection of the plot indicates that it is very closely fit by the thick-film solution of the diffusion equation at low Ag concentrations.
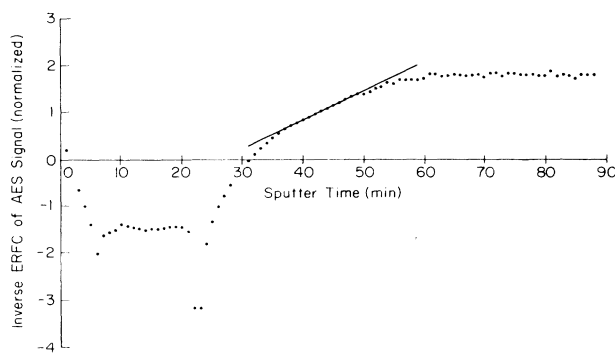

FIG. 4. Plot of the inverse complementary error function of the Ag concentration (normalized to 2) at the Ag/Cu-Zr interface of a sample which was not annealed. The linearity of the midsection of the plot indicates that, as with the annealed samples, it is very closely fit by the thick-film solution of the diffusion equation at low Ag concentrations.

that of Cu, Zr, or the O surface impurity. The Ag profiles from an unannealed sample and another sample following a diffusion anneal of 300 min at the lowest temperature studied, 317 °C, are displayed in Fig. 2. The broadening of the Ag profile following the diffusion anneal is obvious. The abscissa in both figures is the sputter time, which, allowing for slight variations in sputtering rate with changes in composition, is proportional to distance from the initial surface.

Figure 3 is a plot of the inverse complimentary error function of the Ag concentration in an annealed sample (normalized) as a function of the sputter time, showing that there is an extensive straight-line region in which the thick-film solution to the diffusion equation is a good fit to the data. Profiles of unannealed samples are also of this form, as shown in Fig. 4, due to room-temperature diffusion and other effects discussed below. Values of

the Ag diffusion coefficients were calculated from the slopes of the straight-line segments of these plots, after calibration of the sputter-time measurement in terms of an equivalent true distance scale. It should be noted that the straight-line segments correspond to regions of very low Ag concentration, as might be expected.

Table I shows the values of the diffusivities, activation energies, and preexponential factors measured for Ag diffusion for the top side (slow-cooled side) of the specimens and for the wheel side (fast-cooled side). An Arrhenius plot of the Ag diffusion data is shown in Fig. 5. The diffusion coefficients measured for the fast-cooled side of the samples appear to be significantly higher than those for the slow-cooled side.

Auger electrons are emitted only from the topmost 5 Å of a sample. Consequently, the depth resolution of AES is limited by mixing of the top layers of a sample

TABLE I. Diffusion of Ag in amorphous $Cu_{50}Zr_{50}$.

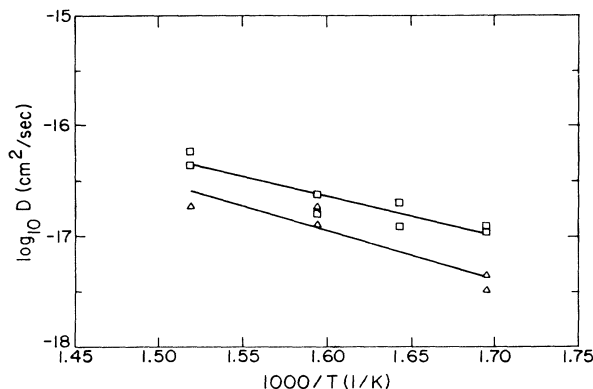| T (°C)	t (min)	D (cm²/sec)	D_0 (cm²/sec)	Q (eV/atom)
Wheel side diffusion				
317.0	300	1.08×10^{-17}	1.30×10^{-11}	0.72
		1.21×10^{-17}		
335.7	300	1.98×10^{-17}		
		1.21×10^{-17}		
354.3	60	2.34×10^{-17}		
		1.58×10^{-17}		
385.4	25	5.81×10^{-17}		
		4.36×10^{-17}		
Top side diffusion				
317.0	300	3.22×10^{-18}	1.18×10^{-10}	0.82
		4.44×10^{-18}		
354.3	60	1.27×10^{-17}		
		1.85×10^{-17}		
385.4	25	1.85×10^{-17}		

FIG. 5. Arrhenius plot of the diffusion coefficient, D, for Ag in the wheel side ($\square$) and the top side ($\triangle$) of melt spun amorphous $Cu_{50}Zr_{50}$. The activation energy and preexponential for Ag diffusion are 0.72 eV/atom and 1.30×10^{-11} cm^2/sec for the wheel side of the glass, and, for the top side, 0.82 eV/atom and 1.18×10^{-10} cm^2/sec.

by the ion beam used for sputtering. At very low sputtering rates, the depth resolution of this technique is approximately 20 Å.

Calculation of diffusion coefficients is complicated by broadening of concentration profiles by the measurement technique used: A step function in concentration is broadened to the inherent depth resolution of the measurement process, and, in general, the measured concentration of an element as a function of depth is the convolution of the actual concentration with the instrumental broadening.

Instrumental broadening arising from small random errors can be modeled as a Gaussian. The convolution of a Gaussian with variance σ_1^2 and another with variance σ_2^2 results in a broader Gaussian with variance σ_T^2 equal to the sum of σ_1^2 and σ_2^2.

If an error function, erf, or complementary error function is convoluted with a Gaussian, the error function is broadened in the same fashion. Diffusion can also be viewed simply as a source of Gaussian broadening. The measured concentration in a sample after a diffusion anneal is the convolution of the actual concentration before annealing and a Gaussian with variance σ_A^2, given by

$$\sigma_A^2 = \sigma_D^2 + \sigma_1^2 + \sigma_2^2 + \cdots , \quad (1)$$

where σ_D is the standard deviation of the broadening due to diffusion, and σ_1, σ_2, etc., are the standard deviations of random errors associated with the measurement process, such as the mixing of atoms at the surface of a sample during sputtering while making a depth profile by AES, the energy width of the He ion beam used for analysis by RBS, surface roughness, room-temperature diffusion that occurred prior to concentration profiling, etc.

Measurement of the concentration profile for the unannealed sample is, of course, subject to the same random and systematic errors involved in measurements made on diffused samples. Designating the broadening of the former by σ_U,

$$\sigma_U^2 = \sigma_1^2 + \sigma_2^2 + \cdots . \quad (2)$$

The broadening due to diffusion alone is given by the difference

$$\sigma_D^2 = \sigma_A^2 - \sigma_U^2 . \quad (3)$$

The diffusion broadening, σ_D, can be equated to the root-mean-square diffusion distance, $(2Dt)^{1/2}$. If the measured concentrations of annealed and unannealed samples are both fit by Gaussians or error functions corresponding to the thin-film or thick-film solutions to the diffusion equation, the values of σ derived from the shape of the concentration profiles can be substituted directly into Eq. (3) to solve for σ_D.

With AES, concentration profiles must be converted from units of sputter time to actual depth below the initial interface in order to calculate absolute values for the diffusion coefficients and preexponential factors. The determination of activation energies, however, is independent of the considerable errors introduced in this calibration. Thus errors involved in determination of activation energies by AES (and by RBS) are significantly less than the errors in the individual values of diffusivity and much less than the errors involved in the preexponential factors. Estimates of the actual errors involved in the present measurements will be given later in this section.

The sputtering rate can be expected to vary somewhat with composition of the sample, but in the limit of low Ag concentration, where the best fit was obtained to the thick-film solution to the diffusion equation, the sputtering rate should be roughly constant and equal to that for zero Ag concentration. The sputtering rate could not be calibrated directly for the melt-spun samples because of unavoidable residual surface roughness. Instead, the rate was calibrated for an evaporated amorphous sample of $Cu_{49}Zr_{51}$ and found to be 5.7 Å/min; this value was used to calculate the values of D displayed in Table I and the figures.
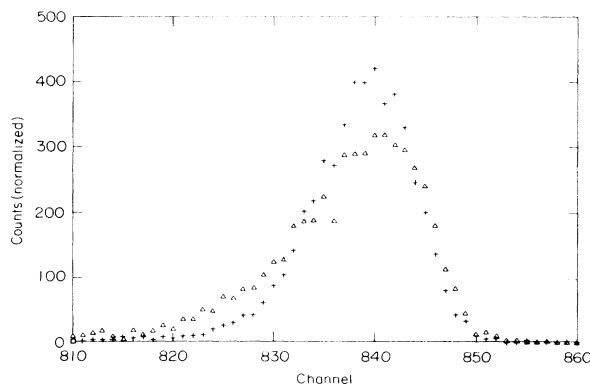

FIG. 6. Comparison of the Au peaks measured by backscattering from the less rapidly quenched side of an unannealed sample of amorphous $Cu_{50}Zr_{50}$ ($+$) and a sample which was annealed at 317.0 °C for 300 min ($\triangle$), showing diffusion of the initial 40-Å thick Au coating into the samples.
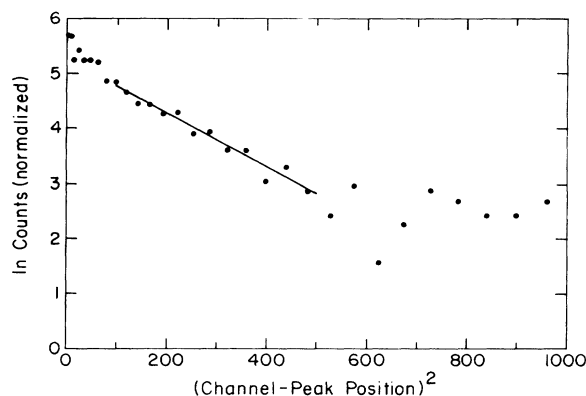
FIG. 7. Natural log of the low-energy side of the Au peak from a sample which was annealed for 300 min at 317.0 °C. The abscissa corresponds to the square of depth measured from the surface of the sample. The linearity of the curve indicates the Au concentration can be fitted to the thin-film solution of the diffusion equation. The fitted segment corresponds to a region of low Au concentration.

B. Au diffusion

The Au peaks from the RBS spectra of an unannealed sample and a sample which was annealed for 300 min at 317 °C are shown in Fig. 6. The low-energy side of the Au peak (smallest Au concentration) from the slow-cooled side of the samples can be fitted to the thin-film solution of the diffusion equation, as shown in Figs. 7 and 8. Direct comparison of broadened and un-broadened peaks is possible because, for the very small beam penetration distances involved, the energy loss of the incident He ions can be assumed to be linear with depth and the scattering cross section of the Au atoms can be assumed to be constant. Unfortunately, measure-

FIG. 9. Au peaks from the most rapidly quenched side of an annealed and unannealed sample of amorphous $Cu_{50}Zr_{50}$, showing anomalous behavior.

ments from the fast-cooled side of the samples could not be accurately fitted to solutions of the diffusion equation. As shown in Fig. 9, the Au peaks from the fast-cooled side of the samples indicate that surface segregation may have occurred during annealing.

Table II shows the diffusivities, activation energy, and preexponential factor measured for Au diffusion in the amorphous alloy for the slow-cooled side of the samples. An Arrhenius plot of these data is shown in Fig. 10. Using values appropriate to $Cu_{50}Zr_{50}$ in the surface energy approximation,[8,11] [S_0], which relates the depth at which a particle is backscattered to the energy loss of the detected particle, is estimated as about 91.8 eV/Å. From calibration measurements made with Al, the energy width per channel is 2.7 keV, and the conversion factor is 29.4 Å/channel. This value has been used to calculate the diffusion coefficients and preexponential factors given in Table II and the figures.
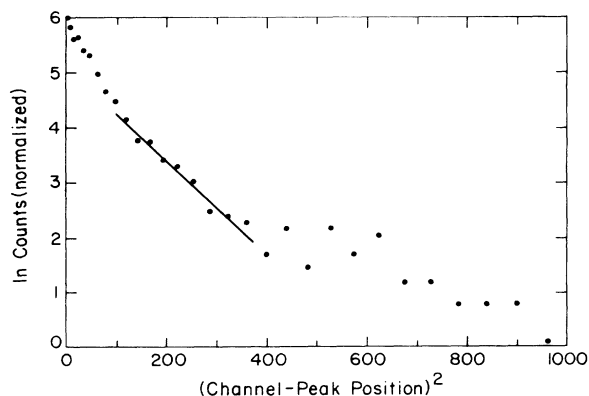

FIG. 8. Natural log of the low-energy side of the Au peak from an unannealed sample. The abscissa corresponds to the square of depth measured from the surface of the sample. The linearity of the curve indicates that the Au concentration can be fitted to the thin-film solution of the diffusion equation, as with the annealed sample.
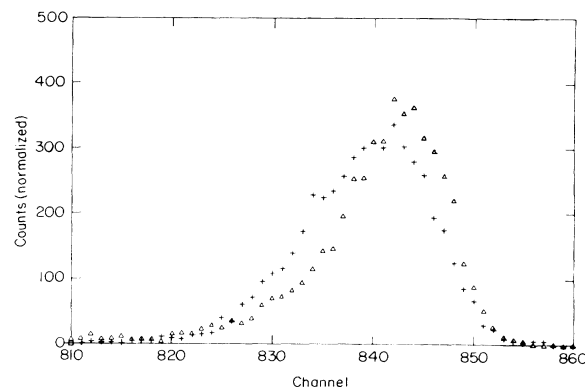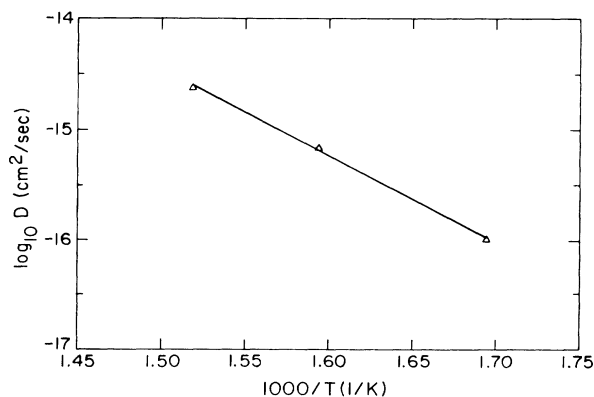

FIG. 10. Arrhenius plot of the diffusion coefficient, D, of Au in the less rapidly quenched side of melt spun amorphous $Cu_{50}Zr_{50}$. The activation energy and preexponential for Au diffusion are 1.55 eV/atom and 1.70×10^{-3} cm²/sec.

TABLE II. Diffusion of Au in amorphous $Cu_{50}Zr_{50}$.

T (°C)	t (min)	D (cm²/sec)	D_0 (cm²/sec)	Q (eV/atom)
		Top side diffusion		
317.0	300	1.05×10^{-16}	1.70×10^{-3}	1.55
354.3	60	7.00×10^{-16}		
385.4	25	2.44×10^{-15}		

C. Errors in diffusion measurements

The present experiment pushes diffusion measurements close to the limits of resolution of current microanalytical techniques, and the experimental errors, accordingly, are much larger than those involved in conventional radiotracer diffusion measurements. Significant errors are unavoidably introduced in calibration of the sputter-time scale (for AES) and energy scale (for RBS) in terms of absolute distance. It should, however, be noted that these errors are not of concern in intercomparison of diffusion measurements made by means of the same technique, nor in calculation of activation energies.

Additionally, since Ag-coated and Au-coated samples were diffused simultaneously, the intercomparison of Ag and Au diffusivities at the same temperature is insensitive to possible random errors in measurement of diffusion time or temperature, but is sensitive to other possible random and relative systematic errors, as discussed later. When the present results are compared with those of other workers, however, all possible errors in these experiments (as well as in the others) must be considered. Principal sources of error are listed in the following.

(1) Measurements of diffusion temperature: Errors may enter due to uncertainties in the thermocouple calibration or readings, or due to thermal gradients over the length of the samples. The last were minimized by sealing the samples under Ar gas to ensure adequate thermal contact and, during the diffusion anneal, enclosing them inside a massive preheated stainless-steel block in the annealing furnace. Temperature errors (maximum) of the order of 1 °C would introduce errors of 3% in D and 6% in activation energies.

(2) Measurements of diffusion time: The principal error in diffusion time arises from uncertainties in the short time interval required for a sample, after insertion into the furnace, to reach equilibrium at the temperature of the block. A direct measurement of this warmup time was not feasible, since the heat conducted to a dummy sample within a small ampoule via sealed-in thermocouple wires would have grossly perturbed the measurement. A calculation for a model air-quartz-argon interface of geometry comparable to that of the real ampoule and sample indicates that the sample should have come to within 15° of the equilibrium temperature within less than 8 sec. Allowing an uncertainty of as large as 2 min in the shortest time interval involved, 25 min at the

highest temperatures, would only introduce an error of 8% in D.

(3) Measurements of diffusion distance and data fitting: By far the most serious of the possible random and systematic errors in this experiment arise from major uncertainties in the actual values of the (extremely small) diffusion penetration distances involved, and, for the Au diffusion measurements, in fitting the raw data to the expected thin-film solutions to the diffusion equation.

In the analysis of the Au diffusion data, the least-squares errors of 10–20 % indicated by the scatter of the data points around the straight-line regions, as shown in Figs. 7 and 8, represent only a small portion of the uncertainty. Additional possibly large but, unfortunately, unquantifiable errors may enter through treatment of the measured profile as a Gaussian and selection of the "best-fit" regions: As evident in Figs. 7 and 8, the "signal" of the enhanced Au concentration in the low-Au-concentration "tail" of the peak is clearly just barely above the "noise" background of the undiffused sample.

Major uncertainties also enter into the calibration of the sputter-time scale (for AES) and energy scale (for RBS) in terms of absolute distance. The surface of the melt-spun samples was too rough to permit direct measurement of the depth of the sputter pits produced during the AES measurements. A calibration measurement was made by sputtering a pit on the flat surface of an evaporated sample of $Cu_{49}Zr_{51}$. This 2500-Å deep pit could be measured to an accuracy of about 100 Å, so that the sputter-time-distance calibration factor was determined, in principle, to 4% uncertainty limits. In fact, the impossibility of aligning the sputtering beam precisely perpendicular to the irregular sample surface and other factors introduced additional larger errors, estimated at 15%.

The distance-scale calibration for the RBS measurements was complicated by the varying Au concentration in the near-surface region of the actual diffusion samples. The calibration is required to establish the absolute value of the energy-loss factor $[S_0]$. If a region of pure Au is assumed as a limiting case, then, from known values of the energy loss of He+ ions in Au, $[S_0]$ would be greater than the value calculated for a dilute solution by a factor of about 1.4, which would eventuate in an underestimation of D by about 30%. The absolute value of $[S_0]$ for pure amorphous $Cu_{50}Zr_{50}$ is not, of course, known from prior direct measurements.

It is difficult to establish quantitative limits of error for the present experiment, particularly since the largest
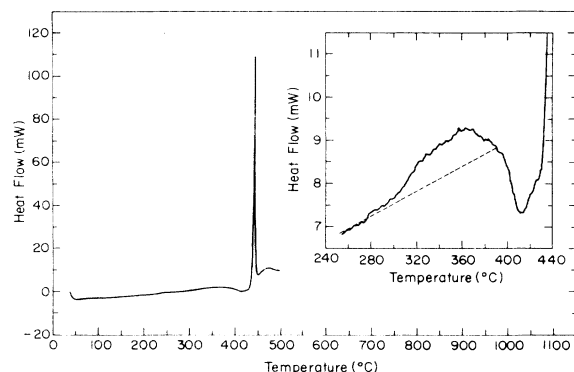
FIG. 11. DSC trace of the crystallization of amorphous $Cu_{50}Zr_{50}$ at a heating rate of 20 °C/min. The inset shows the exothermal plateau that begins over 100 °C below the crystallization peak. At this heating rate, the crystallization temperature, T_x, is 452.2 °C, and the temperature at which the plateau is established, T_p, is 336.8 °C.
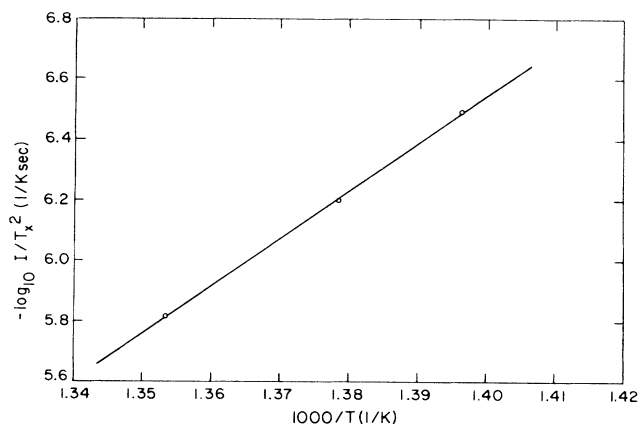
FIG. 12. Kissinger plot of crystallization peak temperatures, T_x, and corresponding heating rates, I. The slope of the linear fit to the data gives an activation energy for crystallization of 3.10 eV/atom.

of these may, in fact, arise from unspecifiable errors involved in fitting the raw data to the mathematical solutions to the diffusion equation. Our best estimate is that Ag diffusivities at the same temperatures may be intercompared within error limits of 30%, and that the uncertainty in the activation energies is within 35%. For comparison of the Ag diffusivities with those determined by other workers, another 20% should be added to the uncertainty, reflecting errors in depth-scale calibration and measurement of annealing time and temperature. For Au diffusion, the estimated error limits are a factor of 2 for D and 50% for activation energies.

D. Thermal measurements

Figure 11 shows the heat evolved from amorphous $Cu_{50}Zr_{50}$ on heating at a constant rate of 20 °C/min. The main peak, arising from crystallization of the sample, is preceded by an exothermal plateau, shown on a magnified scale in the inset.

At a heating rate of 20 °C/min, the plateau forms at 336.8 °C, and the maximum of the crystallization peak occurs at 452.2 °C. Table III shows the temperature of the crystallization peak and that of the onset of the plateau for heating rates of 10 °C/min, 20 °C/min, and 50 °C/min. These data are displayed in a Kissinger plot in Fig. 12 for the crystallization peaks and in Fig. 13 for the plateau regions. From the slopes, the activation en-

TABLE III. Temperatures of exothermal plateau formation and crystallization for amorphous $Cu_{50}Zr_{50}$.

Heating rate (K/min)	Plateau temperature (K)	Crystallization temperature (K)
10	582.5	716.2
20	610.0	725.4
50	640.7	738.9

ergy for crystallization is 3.1 eV/atom, and for the process giving rise to the plateau region, 0.78 eV/atom, nearly the same as that measured for Ag diffusion.

The DuPont 910 DSC apparatus was calibrated by measuring the melting points and enthalpies of fusion of pure In, Sn, and Zn at a heating rate of 20 °C/min. The corrected temperatures were within 0.5 °C of accepted values, and the enthalpies of fusion were measured within 3% of known values. Since the samples and calibration metals were all nominally 15 mg in weight and are of comparable heat capacities, the errors involved in the sample measurements should have been the same as those in the calibration measurements. These would effect an uncertainty of 2% in the activation energy for the plateau region and 5% in the energy for crystallization.
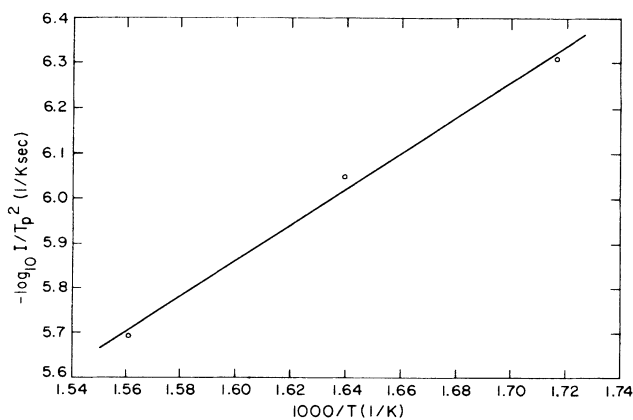
FIG. 13. Kissinger plot of plateau temperatures, T_p, and corresponding heating rates, I. The slope of the line fitted to the data gives an activation energy of 0.78 eV/atom for the process responsible for the appearance of the plateau.

IV. DISCUSSION

A. Diffusion measurements

1. Comparison with earlier diffusion measurements in M-M glasses

The values of diffusivity determined in the present experiment are comparable to those found in studies of other metal-metal glasses at comparable temperatures,[1] as indicated in Fig. 14. The activation energies are also similar: The energy reported for Au diffusion in $Ni_{59.5}Nb_{40.5}$ is 1.0 eV/atom.[3] This alloy, like $Cu_{50}Zr_{50}$, has been shown by neutron and x-ray measurements to have a nearly ideal random structure.[7,8,12] In glasses such as $Ni_{64}Zr_{36}$ and $Ni_{33}Zr_{67}$, which show evidence of short-range order,[13] higher activation energies for Au diffusion, around 1.9 eV/atom, have been reported.[4,5]

The diffusivities of Cu and Ni in $Ni_{50}Zr_{50}$ were found to be greater than that of Au in this material, $Ni_{64}Zr_{36}$, and $Ni_{33}Zr_{67}$,[6] as shown in Fig. 14. The energy for Ni diffusion was found to be approximately 1.1 eV/atom. In general, as was found for Ag and Au in $Cu_{50}Zr_{50}$, solute atoms that are dissimilar to the solvent matrix diffuse more rapidly than atoms which are similar to the matrix.[5] The behavior of the NiZr alloys may be due to the presence of short-range order, which may increase the activation energy for diffusion of the larger Au atoms significantly above that for smaller Cu and Ni atoms.

2. Comparison with self-diffusion in pure copper

A comparison of the present results with bulk self-diffusion in crystalline and liquid copper is shown in Fig. 15.[14-16] The atom packing in the fcc lattice of pure copper is similar to that of the distorted tetrahedra in the $Cu_{50}Zr_{50}$ glass, and the average nearest-neighbor distances are essentially the same: 2.55 Å for Cu and 2.53 Å for $Cu_{50}Zr_{50}$.[8] Extrapolations of the diffusivities of Ag and Au from high-temperature measurements in crystal-

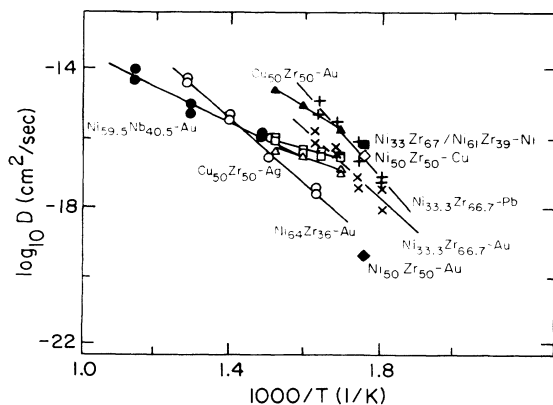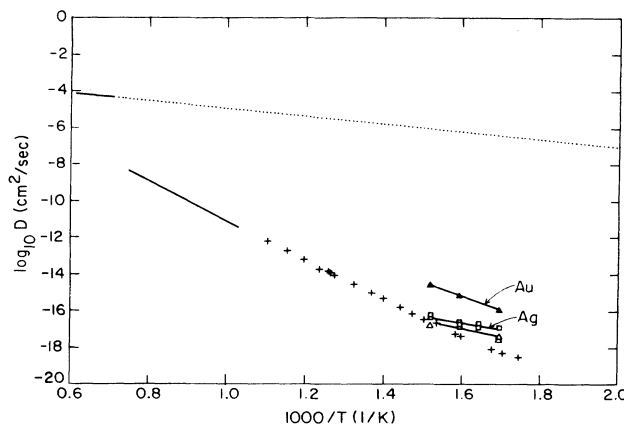FIG. 15. The diffusion of Ag and Au in amorphous $Cu_{50}Zr_{50}$, compared with Cu self-diffusion: High-temperature self-diffusion measurements in crystalline and liquid Cu are shown by (——) (Refs. 14 and 15); (· · · ·) is the extrapolation to low temperatures of self-diffusion in liquid Cu; and (+) is a low-temperature measurement of Cu self-diffusion in a single crystal (Ref. 16).

line Cu (Refs. 17 and 18) show values close to those measured for amorphous $Cu_{50}Zr_{50}$ in this study. Some important features may be noted in the following.

(a) The diffusion coefficients for the amorphous alloy are somewhat higher, but close (within an order of magnitude) to that for crystalline Cu at the same temperatures.

(b) The diffusion coefficients are several orders of magnitude smaller than might be inferred by extrapolation from the liquid state.

(c) The activation energies measured for diffusion in the glass are much closer to that for diffusion in the liquid metal, 0.42 eV/atom,[15] than that for the crystalline solid, 2.19 eV/atom.[14]

Thus it can be concluded that the diffusivity in the amorphous alloy is not very much enhanced either by the (slightly) more open structure in the amorphous alloy or by any strong driving force tending to convert the structure to that of a crystalline solid. Nor is there support for any model in which it is presumed that diffusion occurs without formation of defects (i.e., in which a vacancy or interstitial is provided "free" by the more open structure) and that only motional energy must be provided from the thermal reservoir. Such a model would predict far higher values of the diffusivity.

A more consistent basis for interpretation of the results is by assumption that the amorphous structure is basically stable and that the rate of diffusion is governed largely by the jump distance and the local environment, which in some ways are very close to those for the crystalline solid. The defect involved in the amorphous structure must, however, be different from the simple monovacancy which has been shown to govern diffusion in the crystal, since the sum of its formation and motion energies is less than half that for the monovacancy. As described below, there is other evidence which supports the idea that an extended defect may be responsible for

FIG. 14. Arrhenius plot of Ag and Au diffusion in amorphous $Cu_{50}Zr_{50}$ and diffusion in other metal-metal glasses (Ref. 1).

diffusion in the amorphous structure and that it is very complex, involving a large number of neighboring atoms.

3. Preexponential terms

As noted, the activation energies found for diffusion of Ag and Au in amorphous $Cu_{50}Zr_{50}$ are far smaller, by a factor of around 2 or more, than those typical of diffusion by monovacancies in crystalline Cu. At the same time, the actual values of the diffusion coefficients are comparable, within an order of magnitude or so, with those found for the crystalline materials. The corresponding preexponential terms, the D_0's, are concomitantly found to be far smaller by many orders of magnitude than those characteristic of diffusion in crystals.

Activation energies can be determined, in this work, with far greater accuracy than preexponential terms, and small differences in D_0 even as much as an order of magnitude are not of major concern. In this case, however, the differences are found to be as much as 10 orders of magnitude (e.g., comparing D_0 for self-diffusion in Cu, 0.78 cm^2/sec[14], with D_0 for Ag diffusion in the most rapidly quenched side of amorphous CuZr, 1.3×10^{-11} cm^2/sec). Such differences can hardly be traced to routine experimental errors. The diffusion coefficient,

$$D = D_0 \exp(-Q/kT) , \tag{4}$$

can be written as

$$D = cx^2 v_0 f [\exp(S_f + S_m)/k] \exp[-(H_f + H_m)/kT] , \tag{5}$$

where S_f, S_m and H_f, H_m are the entropies and enthalpies of defect formation and motion.

The preexponential factor is the product of five terms, described below, so that a major change in D_0 must be traceable to large changes in one or more of these terms. The terms may be examined one by one as follows.

(1) The constant c. This term is entirely geometrical in origin and takes account of the number of sites neighboring a diffusing atom. It could not change significantly in going from the crystalline to the amorphous structure.

(2) The mean jump distance x. Since the packing of the amorphous metal is only slightly less dense than that of the crystal, this term, also, could not change appreciably.

(3) The attack frequency v_0. In the crystal, v_0 is usually taken to be of the order of the Debye frequency, 10^{12} to 10^{13} sec^{-1}. This is the frequency at which a single atom would be expected to approach a barrier. If the basic mechanism in the metallic glass also involves the motion of a single atom across a barrier, a comparable attack frequency might be presumed, perhaps smaller by as much as an order of magnitude due to the somewhat expanded structure. On the other hand, if the basic mechanism involves the collective motion of a large number of atoms, a far smaller attack frequency might be expected.

(4) The correlation factor f. This term is model

dependent and would vary between 1, for a completely random jump process, to 0 if no actual transport occurred despite elementary atomic jumps because each jump was followed by a reverse jump, and the motion was completely correlated. The latter would be a completely pathological case, e.g., vacancy diffusion in a one-dimensional lattice. For any reasonable three-dimensional structure and any reasonable mechanism, f would not be expected to vary by more than a factor of 5 or 10 at most. Such small changes cannot account for the present differences.

(5) The entropy term $\exp[(S_f + S_m)/k]$. In crystalline diffusion, S_f and S_m are both small and positive, and the sum is of order $(3-5)k$. such a value is consistent with interstitialcy or monovacancy mechanisms, which are shown by other means to govern diffusion in these structures. To explain the large observed differences between D_0's in crystalline and amorphous structures, the entropy term would have to be large and negative. A negative entropy implies that the basic diffusional step involves, not a single atom, but the collective motion of a large number of atoms. An entropy of, e.g., $-10k$, would be consistent with the "defect" being a complex of a comparable number of atoms, approximately 10.

Accordingly, the large differences in D_0's are most readily explained by changes in items 3 and 5 above, with the assumption that the basic diffusing defect is not a single atom jumping into a vacancy or replacing an interstitial, but is rather a many-atom complex which moves in a complicated, possibly liquidlike fashion through the structure. Such a conclusion is also consistent with the small activation energies found for diffusion, the rate constants associated with crystallization and relaxation, and the relationship between the size of the diffusing atom and the free volume of the glass, discussed below.

4. Diffusion in metallic glasses and the free-volume model

Diffusion in the free-volume model[19-26] occurs when voids which are approximately equal to the volume of the diffusing atom are formed by fluctuations in the distribution of free volume in liquidlike clusters. Structural rearrangement and diffusion both occur via the same mechanism: The viscosity, η, and the diffusion coefficient, D, are given by

$$\eta = \eta_0 \exp(v_m/\bar{v}_{f1}) , \tag{6a}$$

$$D = D_0 \exp(-v_m/\bar{v}_{f1}) , \tag{6b}$$

where v_m is the volume of an atom or molecule and $\bar{v}_{f1}$ is the average free volume available to each atom in a liquidlike cell. If a Lennard-Jones potential is assumed,

$$\bar{v}_{f1} = (k/2\xi_0)\{(T-T_0) + [(T-T_0)^2 + 4v_a\xi_0 T/k]^{1/2}\} , \tag{7}$$

where T and T_0 are the temperature of the glass and that of the ideal glass transition, v_a is an arbitrary constant with units of volume, k is Boltzmann's constant,

and ξ_0 is the limit, for a liquidlike cell in an infinite liquidlike cluster, of the slope, ξ, of the linear region of the cell free energy versus volume curve shown in Fig. 16.[22] For $T \gg T_0$, which yields the experimentally observed temperature dependence for the viscosity and the diffusion coefficient,[23]

$$\bar{v}_{f1} = kT/2\xi_0 . \tag{8}$$

Substituting this into Eq. (6b) gives

$$\xi_0 = Q/2v_m , \tag{9}$$

where Q is the activation energy for diffusion. Using the present values for Q for Ag diffusion and the atomic volume of singly ionized Ag, the slope, ξ_0, is estimated as about 4.5×10^{-2} eV/$\mathring{A}^3$, which, for a typical temperature of 620 K, corresponds to an average free volume per atom of roughly 0.6 $\mathring{A}^3$ in the liquidlike cells. A similar calculation for Au results in an average free volume per atom of approximately 0.4 $\mathring{A}^3$.

Large clusters of liquidlike cells can be expected to contribute more to diffusion than small clusters. The average number of atoms in each liquidlike cluster, weighted by the contribution that the cluster makes to diffusion, is therefore roughly equal to the total amount of free volume in each cluster (of the order v_m) divided by the average free volume per atom, $\bar{v}_{f1}$. Accordingly, the number of atoms in the cluster is of the order

$$v_{Ag}/0.6 \cong 13 . \tag{10}$$

Contributions to the free energy from the configurational entropy make large clusters much more probable than small clusters. Therefore, the cluster size determined from the diffusion measurements may be near to the actual average cluster size. The slope, ξ, of the linear region of the free energy versus volume curve for a single liquidlike cell in a liquidlike cluster is the sum of ξ_0, a constant, and ξ_1, which contains the dependence of ξ on $\bar{v}_{f1}$, and is given by

$$\xi_1 = kT_1/(v_a + \bar{v}_{f1}) . \tag{11}$$

Here T_1 and v_a are arbitrary constants with units of temperature and volume, respectively. If almost all of the clusters in the glass are large clusters, then ξ_1 becomes negligible, and ξ is approximately equal to the value determined for ξ_0.

B. Stability measurements

1. Comparison with other thermal measurements of amorphous Cu-Zr

The crystallization temperatures at heating rates of 10, 20, and 50 K/min, 716.2, 725.4, and 738.9 K, and the activation energy of crystallization, 310 eV/atom, measured in the present study of amorphous $Cu_{50}Zr_{50}$ are in reasonable agreement with previous measurements on amorphous Cu-Zr alloys, as shown in Table IV. The crystallization temperatures in Table IV were determined at heating rates of 10 to 50 K/min and can be expected to differ by approximately 10 K for every increase or decrease in the heating rate by a factor of about 2, varying slightly with the activation energy and the crystallization temperature itself. Higher heating rates result in higher measured crystallization temperatures. The activation energies are determined from the slopes of Kissinger or Bosewell[27] plots of data taken at several heating rates and can be compared without any correction. The scatter in the data is probably due to the presence of impurities and differences in the quenching rates and thermal histories of the samples.

Metallic glasses containing small amounts of impurities are usually more stable than glasses with no impurities. Oxygen contamination of 2 at.% in $Cu_{50}Zr_{50}$ has been shown by Polk et al.[31] to increase the crystallization temperature by roughly 20 K at a heating rate of 80 K/min and to lengthen the incubation time preceding crystallization by a factor of 3 during an isothermal anneal at 700 K. The crystallization temperatures measured in the present study are among the lowest reported, indicating that the samples contain very little oxy-

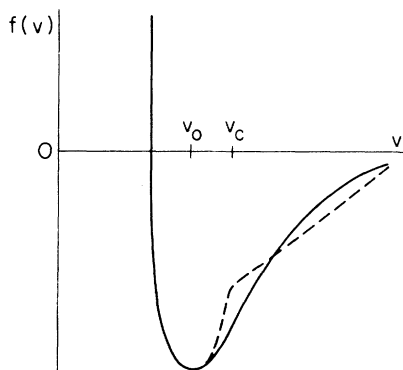FIG. 16. Local free energy $f(v)$ of a cell in the free-volume model. For $v < v_c$, $f(v)$ can be approximated as quadratic and for $v > v_c$, linear in its dependence on v, as shown by the dashed curve (Ref. 22).

TABLE IV. DSC measurements of amorphous Cu-Zr alloys.

Alloy	Crystallization temperature (K)	Heating rate (K/min)	Activation energy (eV/atom)
$Cu_{45}Zr_{55}$	732	50	3.87[a]
	723	50	4.25[b]
$Cu_{48}Zr_{52}$	750	50	4.49[a]
$Cu_{50}Zr_{50}$	790	50	4.11[c]
	790	50	4.21[c]
	730	20	3.17[d]
	725	20	3.10
$Cu_{55}Zr_{45}$	748	20	3.68[d]
	770	50	5.30[b]

[a]Reference 9.
[b]Reference 28.
[c]Reference 29.
[d]Reference 30.

gen. Using this criterion, the most reliable data for amorphous $Cu_{50}Zr_{50}$ are the data of Budhani et al.[30] and the present study.

2. Exothermal effects preceding crystallization

The exothermal plateau in Fig. 11 preceding the crystallization peak is due to the relaxation of the glass and can be interpreted as resulting from processes with a spectrum of activation energies.[32-34] The close agreement between the average activation energy for Ag diffusion, 0.77 eV/atom, and the activation energy associated with the formation of the exothermal plateau, 0.78 eV/atom, indicates that the relaxation of the glass occurs chiefly by diffusion.

Similar exothermal processes have been observed by Harmelin et al.[35] in amorphous Cu_xZr_{1-x} for $x = 0.33$ to 0.60. The effect is irreversible and can be partially reduced or eliminated by annealing. Since the samples used in the present experiment were not annealed, the plateau can be presumed to represent the relaxation processes in the as-quenched material.

3. Crystallization and stability

The crystallization of a metallic glass is believed to be similar to the crystallization of an undercooled liquid.[36-38] At any temperature, a liquid contains solid-like clusters of atoms. Below the melting temperature of the liquid, the free energy of the solid phase is less than that of the liquid, but the formation of crystallization nuclei is restricted by a large positive surface free energy. For a spherical nucleus of radius r, the contribution G_N of the surface and volume terms to the total free energy is

$$G_N = -\tfrac{4}{3}\pi r^3 L(T_m - T)/T_m + 4\pi r^2\gamma , \qquad (12)$$

where γ is the surface or interfacial energy, T_m is the melting temperature, and L is the latent heat of fusion per unit volume. The nucleus is stable when $dG_N/dr = 0$, or

$$r = 2\gamma T_m/L(T_m - T) . \qquad (13)$$

In equilibrium, the number of stable nuclei n at temperature T is given by

$$n = N\exp(-G_N/kT) . \qquad (14)$$

A nucleus larger than the critical radius grows, by diffusion, to form a microcrystal.

The activation energy of crystallization in this model is the sum of the activation energy of diffusion and the activation energy associated with the growth of crystallization nuclei. Using the activation energy of crystallization found by Kissinger's method, 3.10 eV/atom, and assuming that the average activation energy for the diffusion of Ag, 0.77 eV/atom, is similar to the activation energy for self-diffusion in the glass, the activation energy associated with the growth of the crystallization nuclei is roughly 2.33 eV/atom. The enthalpy of crystallization for amorphous $Cu_{50}Zr_{50}$, which can be taken to correspond with the latent heat L in Eq. (12), is

roughly 0.05 eV/atom,[28] the number density is 2.856×10^{22} formula units per cm^3,[8] and the melting temperature is approximately 930 °C.[39] Using these values and Eqs. (12) and (13), at 400 °C, an activation energy of nucleation of 2.3 eV/atom corresponds to a critical radius of 12 Å.

When quenched relatively slowly from the liquid, $Cu_{50}Zr_{50}$ crystallizes into a metastable bcc CsCl structure,[40] in which the Zr atoms are on the corners of the unit cell and a Cu atom is in the center, with a lattice constant of 3.262 Å. If the high-temperature CsCl structure is metastably retained to low temperatures, the alloy undergoes a martensitic transformation at approximately 440 K. A eutectoid transformation to Zr_7Cu_{10} and Zr_2Cu occurs if the CsCl phase is annealed just below 985 K. Buschow[9] found that amorphous $Cu_{50}Zr_{50}$ crystallized into a phase which was tentatively identified as having an orthorhombic unit cell with lattice constants $a = 3.33$ Å, $b = 6.25$ Å, and $c = 15.60$ Å. It was stable after annealing at 600 °C for a week, but decomposed into other Cu-Zr compounds or underwent a structural transformation above 650 °C.

The stability of amorphous $Cu_{50}Zr_{50}$ can most likely be attributed to the large structural differences between the amorphous phase, which is primarily composed of distorted tetrahedra, and the crystalline phase, which may be orthorhombic or bcc. The large difference, roughly 2.3 eV/atom, between the activation energy associated with crystallization and that associated with diffusion indicates that the rate-limiting step in the amorphous-crystalline transition is the formation of finite crystallization nuclei, rather than only the diffusional motion of atoms. In contrast, the stability of metal-metalloid glasses is usually attributed to the short-range order resulting from the presence of metal-loid atoms, which stabilizes the randomly packed amorphous structure even though it is rather similar to the fcc crystalline lattice.

V. CONCLUSIONS

The diffusion coefficients of Ag and Au in amorphous $Cu_{50}Zr_{50}$ are somewhat higher than, but very close in magnitude to, the coefficient of self-diffusion in crystalline Cu at the same temperatures. However, the activation energies for diffusion in the amorphous alloy (0.77 eV/atom for Ag and 1.55 eV/atom for Au) are much less than the activation energy for self-diffusion in crystalline Cu (2.19 eV/atom) and approach that for liquid Cu (0.42 eV/atom). These facts, and the extremely small preexponential factors for diffusion in the amorphous alloy (on the order of 10^{-10} to 10^{-11} cm^2/sec for Ag), indicate that the mechanism for diffusion in the amorphous metal may involve an extended defect rather than the monovacancy dominant in the crystalline solid and, furthermore, that there is not a strong driving force affecting diffusion in the glass.

Comparison with measurements of diffusion in other amorphous metal-metal alloys indicates that the activation energies and preexponentials for diffusion in glasses with almost no short-range order are generally very

small. From the magnitude of the preexponential factors measured for diffusion in amorphous $Cu_{50}Zr_{50}$, the extended defect can be expected to involve 10 or more atoms. Analysis of the data in terms of the free-volume model also lends strength to this conclusion and indicates that the glass is composed of liquidlike clusters of approximately 13 or more atoms, with an average free volume per atom of around 0.6 Å³.

The initial stage of relaxation in amorphous $Cu_{50}Zr_{50}$ occurs with a spectrum of activation energies. The lowest activation energy involved, 0.78 eV/atom, is almost identical to the average activation energy of Ag diffusion in the glass, 0.77 eV/atom, indicating that relaxation occurs primarily through diffusion.

At a heating rate of 20°C/min, crystallization occurs at 452.2 °C. The activation energy of crystallization was found by Kissinger's method to be 3.10 eV/atom. The large difference, on the order of 2.3 eV/atom, between the activation energies for crystallization and diffusion is attributed to the large difference in structure between

crystalline and amorphous $Cu_{50}Zr_{50}$, which can be expected to increase the activation energy for formation of crystallization nuclei. The stability of amorphous $Cu_{50}Zr_{50}$ is probably a result of the difference in structure between the amorphous phase, which consists primarily of distorted tetrahedra, and the crystalline phase, which has either a bcc CsCl structure or is orthorhombic.

ACKNOWLEDGMENTS

*Present address: Research Laboratories, Eastman Kodak Company, Rochester, NY 14650.

[1]B. Cantor and R. W. Cahn, in *Amorphous Metallic Alloys,* edited by F. E. Luborsky (Butterworths, London, 1983), pp. 487–504.

[2]M. Kijek, M. Ahmadzadeh, and B. Cantor in *Conference on Metallic Glasses: Science and Technology,* edited by C. Hargitai, I. Bakonyi, and T. Kemeny (Central Research Institute for Physics, Budapest, 1980), Vol. 2, pp. 397–406.

[3]M. Kijek, D. Akhtar, B. Cantor, and R. W. Cahn, in *Rapidly Quenched Metals,* edited by T. Masumoto and K. Suzuki (Japan Institute of Metals, Sendai, 1982), Vol. I, pp. 573–577.

[4]D. Akhtar, B. Cantor, and R. W. Cahn, Acta Metall. **30**, 1571 (1982).

[5]D. Akhtar, B. Cantor, and R. W. Cahn, Scr. Metall. **16**, 417 (1982).

[6]H. Hahn, R. S. Averback, and S. J. Rothman, Phys. Rev. B **33**, 8825 (1986).

[7]T. Mizoguchi, T. Kudo, and T. Irisawa, in *Rapidly Quenched Metals II,* edited by N. J. Grant and B. C. Giessen (M.I.T. Press, Cambridge, 1976), pp. 384–391.

[8]H. S. Chen and Y. Waseda, Phys. Status Solidi A **51**, 593 (1971).

[9]K. H. J. Buschow, J. Appl. Phys. **52**, 3319 (1981).

[10]H. E. Kissinger, Anal. Chem. **29**, 1702 (1957).

[11]W. K. Chu, J. W. Mayer, and M. A. Nicolet, *Backscattering Spectrometry* (Academic, New York, 1978).

[12]E. Svab, F. Forgacs, F. Hajdu, N. Kroo, and J. Takacs, J. Non-Cryst. Solids **46**, 125 (1981).

[13]Y. Waseda and H. S. Chen, in *Rapidly Quenched Metals III,* edited by B. Cantor (Metals Society, London, 1978), Vol. 2, pp. 415–418.

[14]S. J. Rothman and N. L. Peterson, Phys. Status Solidi **35**, 305 (1969).

[15]J. Henderson and L. Yang, Trans. Metall. Soc. AIME **221**, 72 (1961).

[16]K. Maier, Phys. Status Solidi A **44**, 567 (1977).

[17]C. T. Tomizuka, referred to by D. Lazarus, in *Solid State*

Physics, edited by F. Seitz and D. Turnbull (Academic, New York, 1960), Vol. 10, pp. 71–126.

[18]C. T. Tomizuka, Bull. Am. Phys. Soc. **2**, 123 (1957).

[19]M. H. Cohen and D. Turnbull, J. Chem. Phys. **31**, 1164 (1959).

[20]D. Turnbull and M. H. Cohen, J. Chem. Phys. **34**, 120 (1961).

[21]D. Turnbull and M. H. Cohen, J. Chem. Phys. **52**, 3038 (1970).

[22]M. H. Cohen and G. S. Grest, Phys. Rev. B **20**, 1077 (1979).

[23]R. Zallen, *The Physics of Amorphous Solids* (Wiley, New York, 1983), pp. 212–223.

[24]G. S. Grest and M. H. Cohen, in *Advances in Chemical Physics,* edited by I. Prigogine and S. A. Rice (Wiley, New York, 1981), Vol. 48, pp. 455–525.

[25]G. S. Grest and M. H. Cohen, in *Annals of the Israel Physical Society,* edited by G. Deutscher, R. Zallen, and J. Adler (Adam Hilger, Bristol, 1983), Vol. 5, pp. 187–206.

[26]M. H. Cohen and G. S. Grest, J. Non-Cryst. Solids **61/62**, 749 (1984).

[27]F. G. Boswell, J. Therm. Anal. **18**, 353 (1980).

[28]I. Ansara, A. Pasturel, and K. H. J. Buschow, Phys. Status Solidi A **69**, 447 (1982).

[29]H. J. Eifert, B. Elschner, and K. H. J. Buschow, Phys. Rev. B **25**, 7441 (1982).

[30]R. C. Budhani, T. C. Goel, and K. L. Chopra, in *Rapidly Quenched Metals,* edited by T. Masumoto and K. Suzuki (Japan Institute of Metals, Sendai, 1982), Vol. II, pp. 615–618.

[31]D. E. Polk, C. E. Dube, and B. C. Giessen, in *Rapidly Quenched Metals III,* edited by B. Cantor (Metals Society, London, 1978), Vol. 1, pp. 220–230.

[32]M. R. J. Gibbs, J. E. Evetts, and J. A. Leake, J. Mater. Sci. **18**, 278 (1983).

[33]W. Primak, Phys. Rev. **100**, 1677 (1955).

[34]M. R. J. Gibbs, D. W. Stephens, and J. E. Evetts, J. Non-Cryst. Solids **61/62**, 925 (1984).

[35]M. Harmelin, Y. Calvayrac, A. Quivy, J. Bigot, P. Burnier, and M. Fayard, J. Non-Cryst. Solids **61/62**, 931 (1984).

[36]H. Biloni, in *Physical Metallurgy,* edited by R. W. Cahn and P. Haasen (North-Holland, Amsterdam, 1983), Pt. 1, pp. 483–486.

[37]D. Turnbull, Contemp. Phys. **10**, 473 (1969).

[38]M. Rosen, H. N. G. Wadley, and R. Mehrabian, Scr. Metall. **15**, 1231 (1981).

[39]M. Hansen and K. Anderko, *Constitution of Binary Alloys* (McGraw-Hill, New York, 1958), pp. 655–657.

[40]E. M. Carvalho and I. R. Harris, J. Mater. Sci. **15**, 1224 (1980).